Supplementary Information

Irreversible Electrochemical Reaction at High Voltage Induced by Distortion of Mn and V Structural Environments in $Na_4MnV(PO_4)_3$

Sunkyu Park [1,2,3], Jean-Noël Chotard [1,5], Dany Carlier [2,5], François Fauth [4], Antonella Iadecola [5], Christian Masquelier [*,1,5] and Laurence Croguennec [*,2,5]

[1] Laboratoire de Réactivité et de Chimie des Solides, Université de Picardie Jules Verne, CNRS-UMR 7314, F-80039 Amiens Cedex 1, France

[2] Univ. Bordeaux, CNRS, Bordeaux INP, ICMCB UMR 5026, F-33600 Pessac, France

[3] TIAMAT, 15 Rue Baudelocque, F-80000 Amiens, France

[4] CELLS-ALBA Synchrotron, Cerdanyola del Vallès, E-08290 Barcelona, Spain

[5] RS2E, Réseau sur le stockage électrochimique de l'énergie, FR CNRS 3459, F-80039 Amiens Cedex 1, France

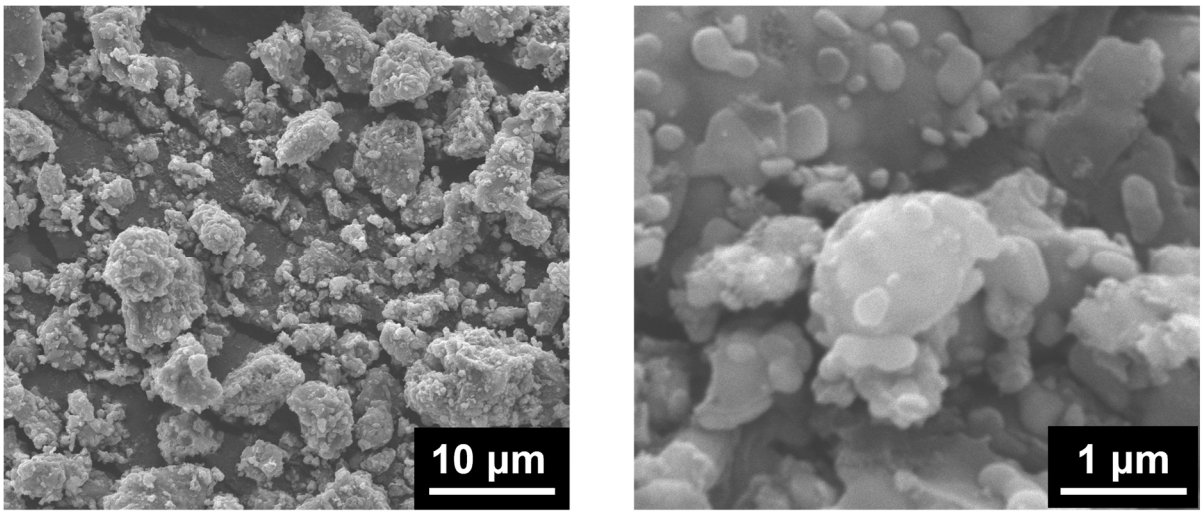

Figure S1. SEM images of $Na_4MnV(PO_4)_3$.

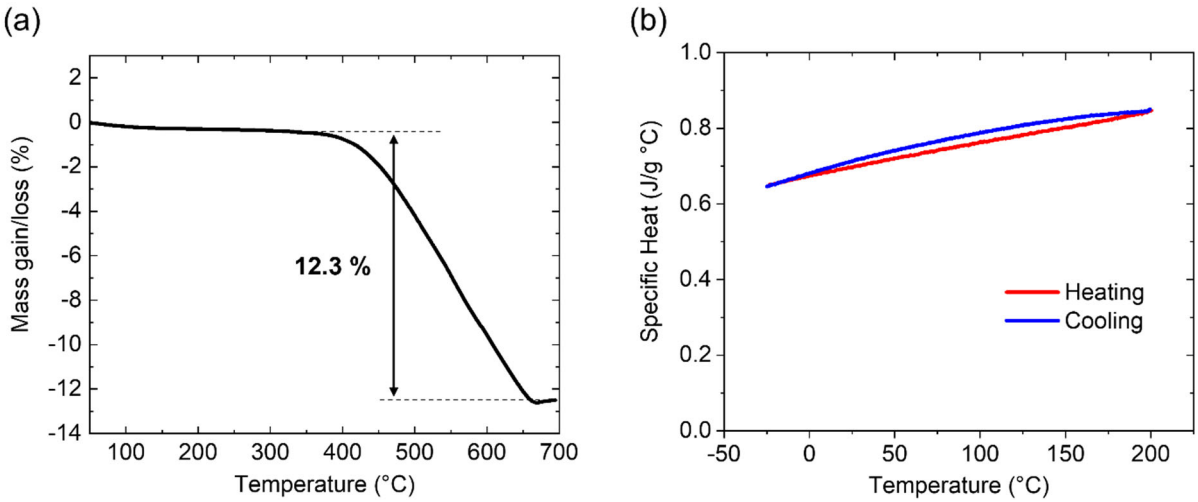

Figure S2. **(a)** TGA data of the $Na_4MnV(PO_4)_3$ powder, measured in air with the heating rate of 10 K/min. **(b)** Adiabatic calorimetry between -25 and 300 °C upon heating and upon cooling.

Table S1. Refined structural parameters of the $Na_4MnV(PO_4)_3$ powder collected within a capillary at 298 K.

$Na_4MnV(PO_4)_3$

Space group: *R*-3*c* (#167); *Z* =6

a = 8.9640(2) Å; *c* = 21.4724(4) Å; *c*/*a* = 2.395

V = 1494.20(2) Å^3; *V*/*Z* = 249.034(8) Å^3

R_{wp} = 16.7 %; R_p = 16.6 %; R_{Bragg} = 8.3 %

Atom	Wyckoff position	x/a	y/b	z/c	Uiso, Å^2	Occ.
Mn/V(1)	12c	0	0	0.1491(2)	0.010(2)	0.5/0.5
P(1)	18e	0.2985(8)	0	0.25	0.015(2)	1
Na(1)	6b	0	0	0	0.021(6)	0.97(3)
Na(2)	18e	0.6420(13)	0	0.25	0.028(5)	0.96(2)
O(1)	36f	0.0144(16)	0.2091(14)	0.1928(5)	0.023(4)	1
O(2)	36f	0.1870(12)	0.1724(13)	0.0842(6)	0.017(3)	1

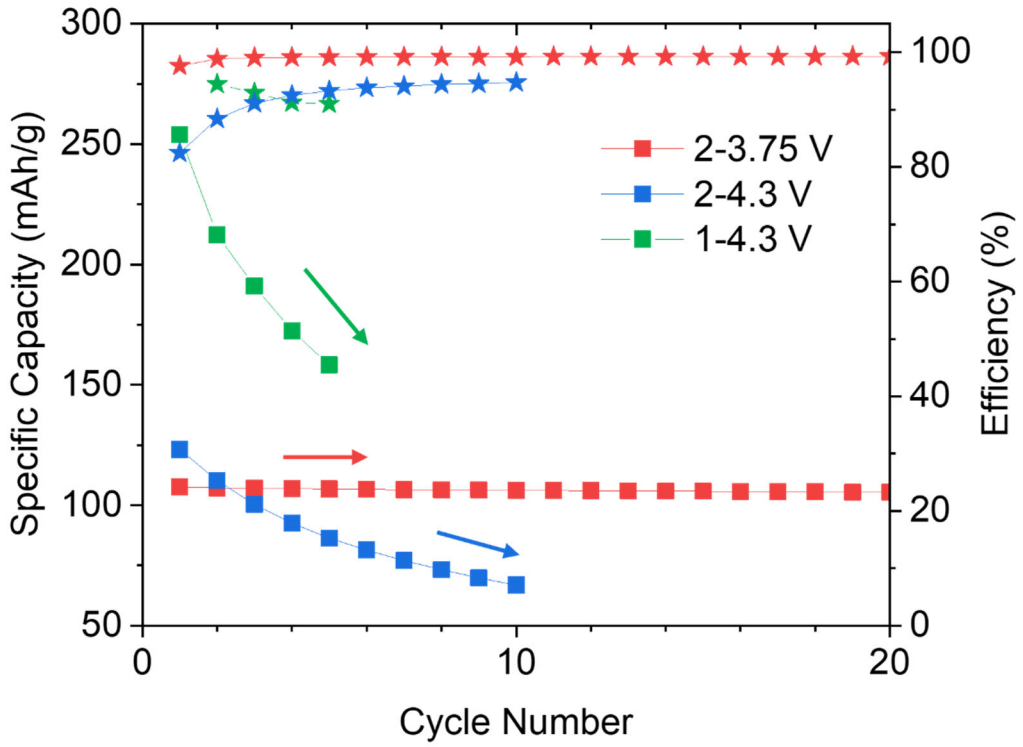

Figure S3. Specific discharge capacity (■) and coulombic efficiency (★) during the first 5-20 cycles in the voltage windows of 2-3.75 V (red), 2-4.3 V (blue), 1-4.3 V (green) at the C-rate of C/10 (1 Na^+ in 10 h).

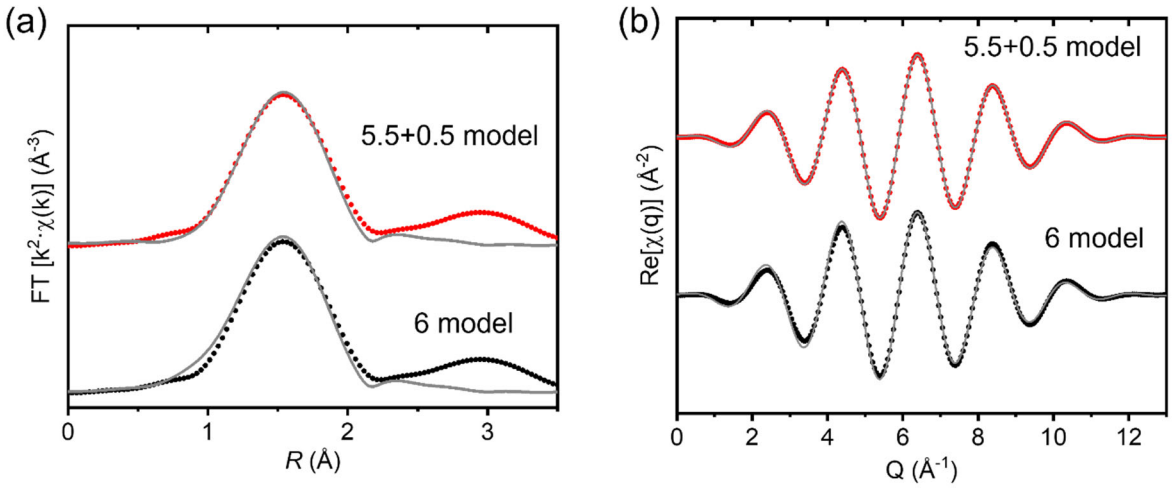

Figure S4. (a) Different coordination models of k^2-weighted Fourier transformed EXAFS oscillations at V K-edge after the first cycle with the voltage window of 2-4.3V. (b) Corresponding backward Fourier transforms in *q*-space.

Table S2. Refined parameters for the first coordination shell of V K-edge EXAFS spectra considering different coordination models for V in $Na_4MnV(PO_4)_3$ recovered after the first cycle with the voltage window of 2-4.3 V: *k*-range: 2.7 - 10.7 $Å^{-1}$, R-range: 1.0 - 2.1 Å, dR = 0, sine window

Coordination model	d(V – O) (Å)	E_0 (eV)	σ^2 ($Å^2$)	R-factor
6	2.014(5) X 6	-0.8	0.0064(5)	0.0150
5.5+0.5	2.013(5) X 5.5 1.645(5) X 0.5	0.5	0.0058(5)	0.0017

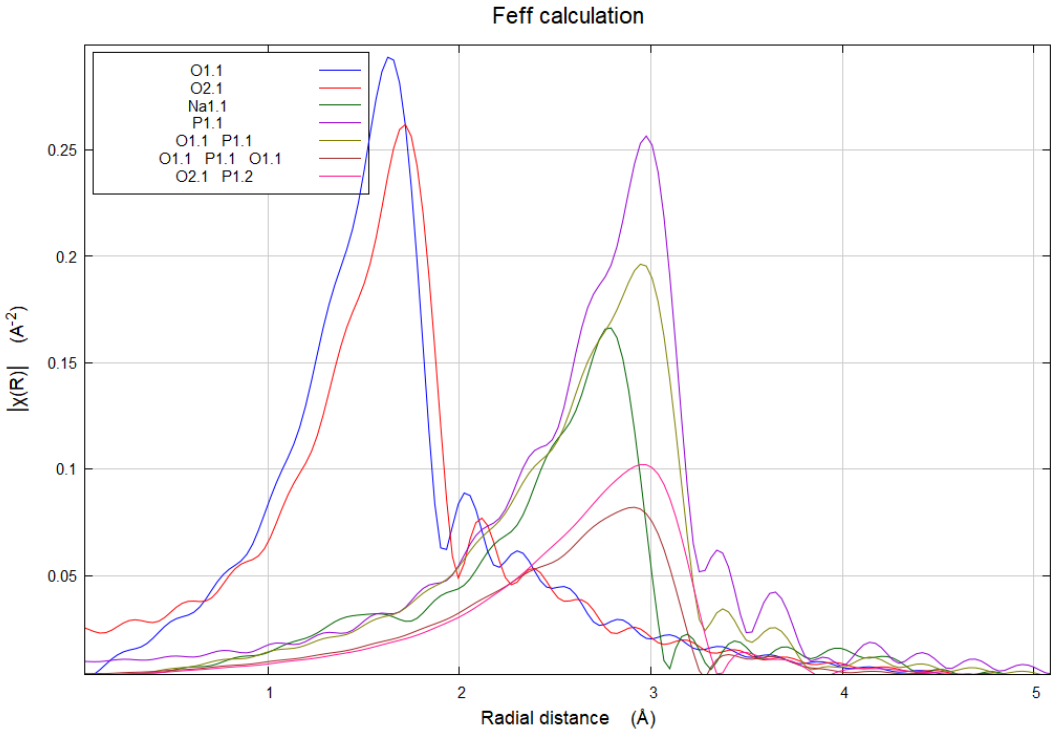

Figure S5. Calculated FT-EXAFS oscillations which are deconvoluted with the various scattering paths for $Na_4MnV(PO_4)_3$ at V K-edge

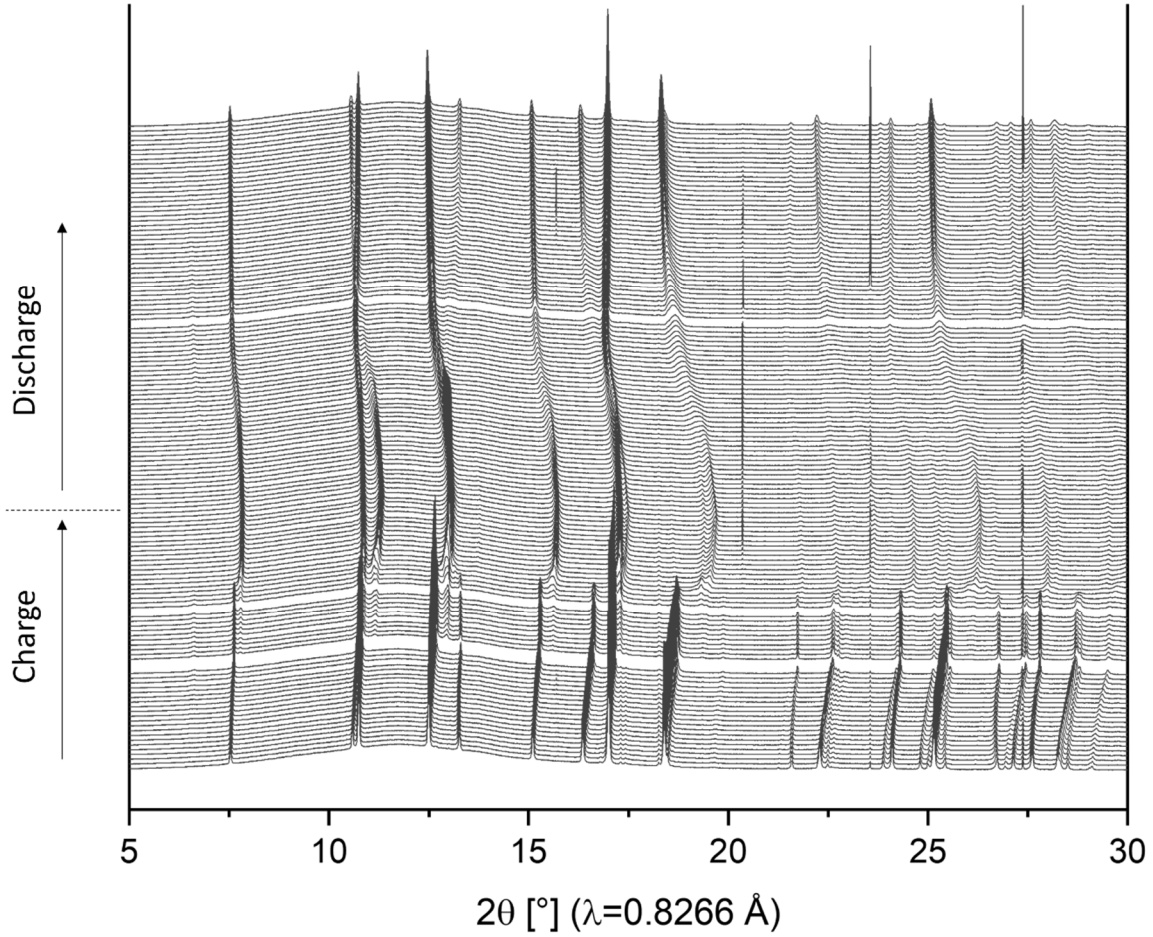

Figure S6. Wider 2θ range synchrotron XRPD patterns collected *operando* during the first cycle of $Na_4MnV(PO_4)_3$ vs. Na metal, within a voltage window of 1.0 – 4.3 V vs. Na^+/Na at the C-rate of C/9 (= 1 Na^+ in 9 h). The same data with the narrower 2θ range are shown in Figure 4.

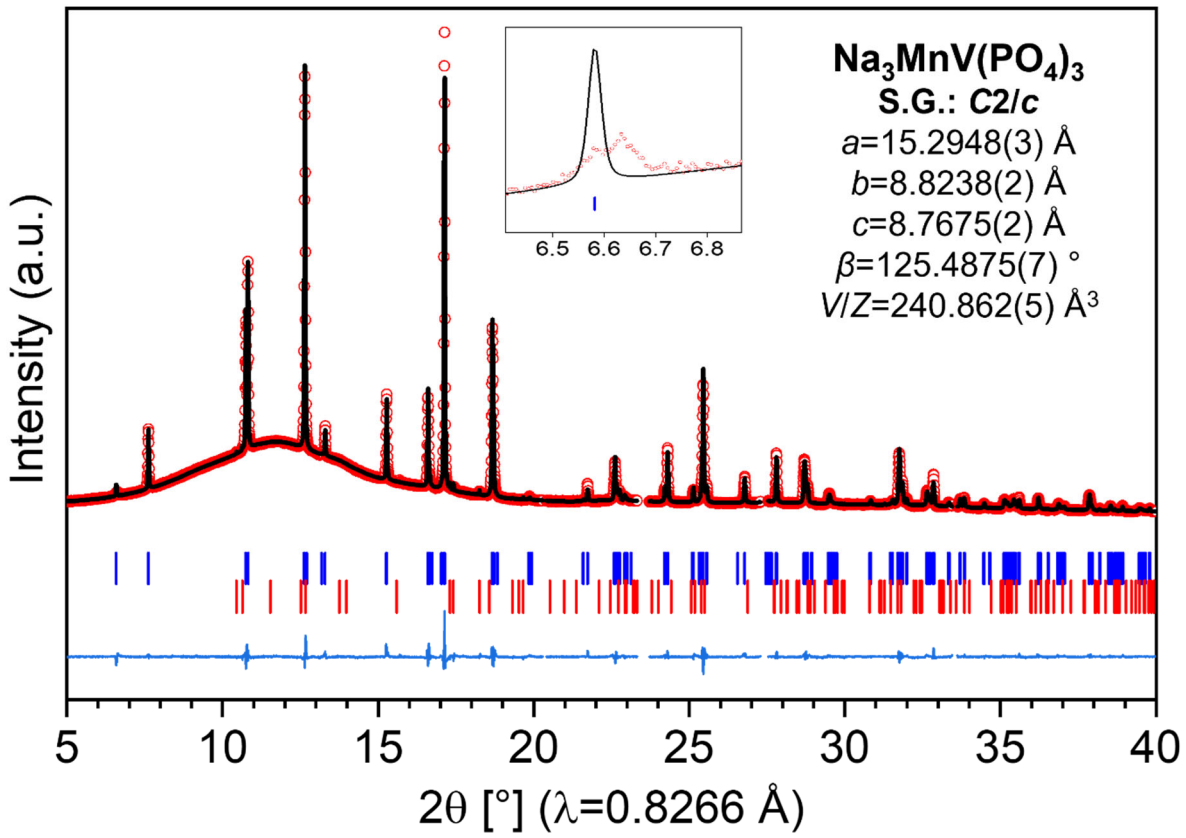

Figure S7. Rietveld refinement results of $Na_3MnV(PO_4)_3$ using the *C*2/*c* space group obtained from the synchrotron XRPD pattern collected with the *in situ* cell during charge.

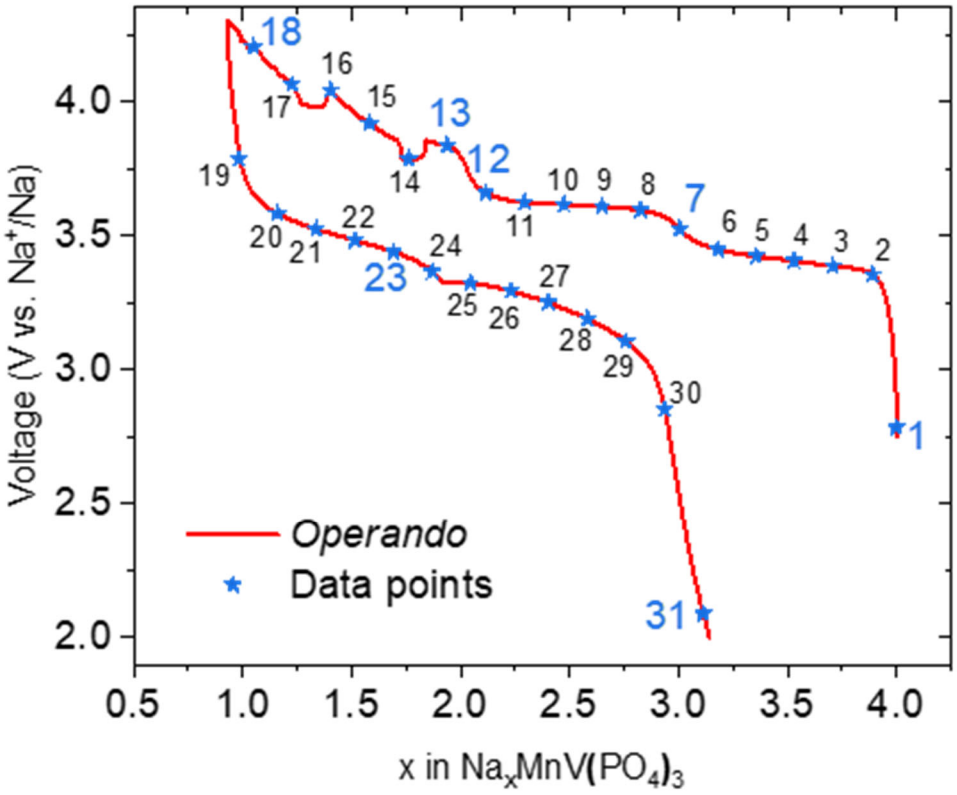

Figure S8. The starting points of the acquisition for each XAS spectrum and the voltage profile obtained with the *in situ* cell for the XAS *operando* measurements.

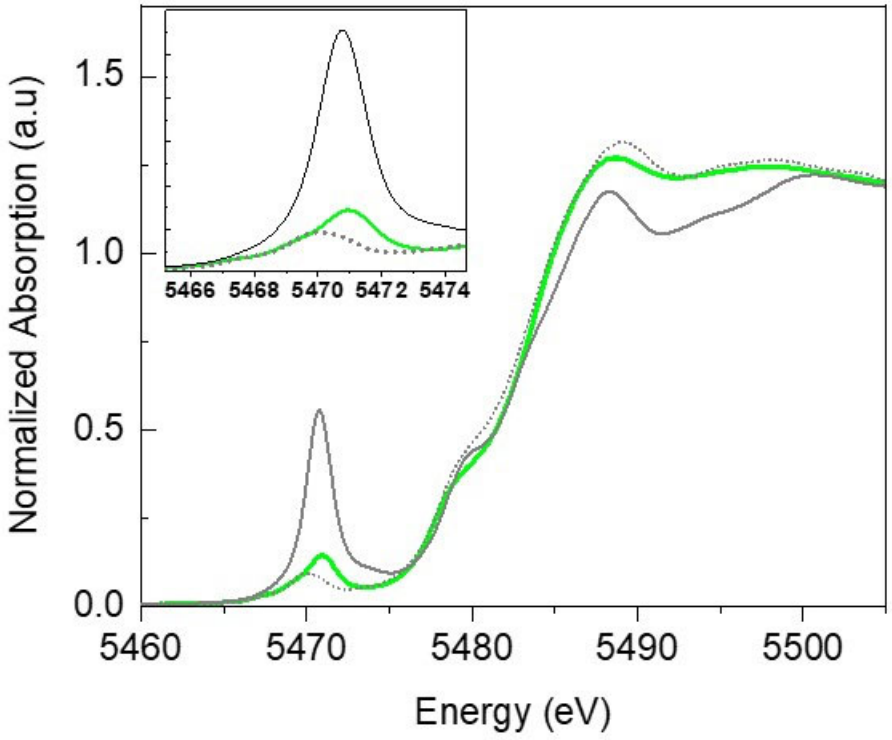

Figure S9. Comparison of the spectrum #18 (end of charge, in green) with those of $V^{5+}OPO_4$ (with vanadyle type bonds, in black continuous line) and $Na1V^{4+}2(PO4)3$ (with V^{4+} in symmetric oxygen octahedra, in black dotted line). As expected for a more distorted environment, the pre-edge is more intense for $VOPO_4$. As expected, the pre-edge position shifts to higher energy when moving from $V^{4+}O_6$ in $Na_1V_2(PO_4)_3$ to $V^{>4+}O_6$ in $Na_{\sim 1}MnV(PO_4)_3$.

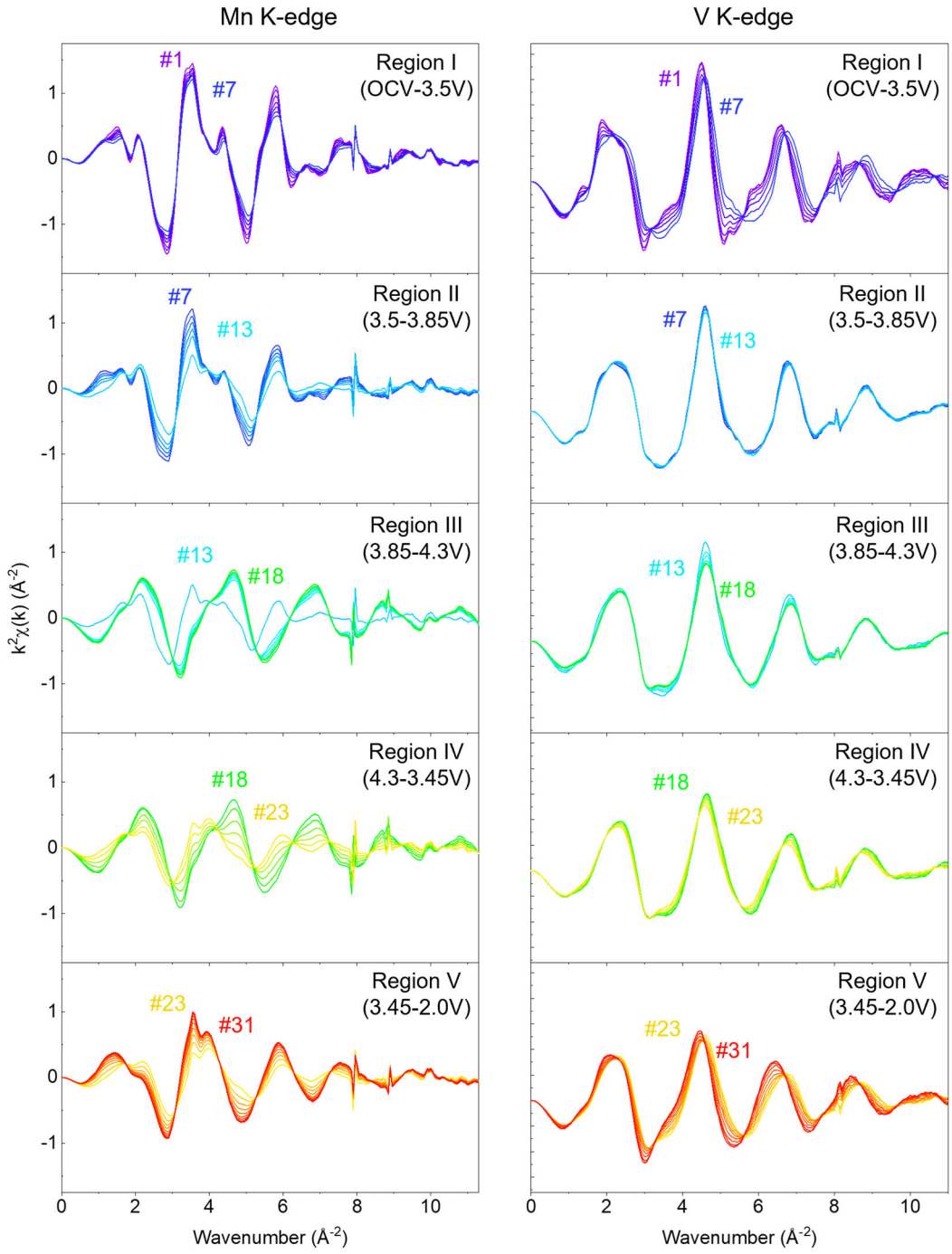

Figure S10. EXAFS oscillations at Mn and V K-edges collected in *operando* conditions at different states of charge and discharge of the battery for the $Na_4MnV(PO_4)_3$ positive electrode. The range of EXAFS oscillations at Mn K-edge was limited due to the presence of Fe in the Be windows of the electrochemical cell.

Table S3. Refined parameters for the first shell of Mn K-edge EXAFS spectra. *k*-range: 2.3 - 11.3 $Å^{-1}$, R-range: 1.0 - 2.1 Å, dR = 0, sine window. The coordination number (N) was set to 6, and attenuation factors (S_0^2) were fixed as 0.887. The Mn – O distances and the Debye-Waller factors (σ_i^2) were refined, whereas the energy shift (E_0) was first refined before being fixed.

Spectrum number	d(Mn-O) (Å)		E_0 (eV)	σ^2 ($Å^2$)	R-factor
1	2.135(5)	-	0.0	0.010	0.0099
2	2.135(5)	-	-0.1	0.011	0.0108
3	2.133(5)	-	-0.2	0.011	0.0110
4	2.119(5)	-	-1.6	0.012	0.0122
5	2.114(5)	-	-2.3	0.013	0.0124
6	2.106(5)	-	-3.1	0.013	0.0123
7	2.098(5)	-	-4.0	0.014	0.0150
8	2.100(5)	-	-3.4	0.016	0.0199
9	2.122(5)	-	-0.3	0.018	0.0315
10	2.121(5)	-	-0.2	0.020	0.0358
11	2.117(5)	-	-0.1	0.023	0.0426
13	1.935(5)	2.236(5)	0.0	0.009	0.0134
14	1.932(5)	2.241(5)	0.0	0.009	0.0151
15	1.931(5)	2.250(5)	0.0	0.008	0.0177
16	1.929(5)	2.256(5)	-0.1	0.008	0.0222
17	1.927(5)	2.273(5)	-0.4	0.008	0.0241
18	1.926(5)	2.240(5)	-0.3	0.009	0.0176
19	1.924(5)	2.207(5)	-0.7	0.011	0.0130
20	1.923(5)	2.206(5)	-1.0	0.011	0.0121
21	1.930(5)	2.197(5)	-2.1	0.015	0.0486
24	2.145(5)	1.949(5)	-0.5	0.012	0.0245
25	2.122(5)	-	1.2	0.020	0.0324
26	2.119(5)	-	0.3	0.018	0.0219
27	2.118(5)	-	0.0	0.016	0.0150
28	2.114(5)	-	-0.7	0.014	0.0113
29	2.113(5)	-	-0.8	0.014	0.0099
30	2.113(5)	-	-1.1	0.013	0.0096
31	2.119(5)	-	-0.1	0.013	0.0086

Table S4. Refined parameters for the first shell of V K-edge EXAFS spectra. *k*-range: 2.7 – 10.7 $Å^{-1}$, R-range: 1.0 - 2.1 Å, dR = 0, sine window. The coordination number (N) was set to 6, and attenuation factors (S_0^2) were fixed as 0.884. The V – O distances and the Debye-Waller factors (σ_i^2) were refined, whereas the energy shift (E_0) was first refined before being fixed.

Spectrum number	d(V-O) (Å)		E_0 (eV)	σ^2 ($Å^2$)	R-factor
1	2.021(5)	-	2.1	0.005	0.0018
2	2.018(5)	-	2.0	0.005	0.0014
3	2.015(5)	-	2.2	0.006	0.0008
4	2.005(5)	-	2.2	0.007	0.0005
5	1.991(5)	-	2.0	0.008	0.0005
6	1.967(5)	-	1.4	0.008	0.0008
7	1.939(5)	-	0.1	0.007	0.0007
8	1.935(5)	-	-0.1	0.007	0.0011
9	1.935(5)	-	0.1	0.007	0.0010
10	1.934(5)	-	0.1	0.007	0.0014
11	1.934(5)	-	0.2	0.007	0.0011
12	1.934(5)	-	0.3	0.007	0.0016
13	1.931(5)	-	0.2	0.007	0.0013
15	1.931(5)	1.652(5)	0.5	0.007	0.0014
16	1.931(5)	1.633(5)	0.5	0.008	0.0016
18	1.930(5)	1.630(5)	0.6	0.007	0.0015
19	1.934(5)	1.610(5)	1.1	0.008	0.0017
20	1.938(5)	1.611(5)	1.1	0.008	0.0017
21	1.944(5)	1.622(5)	1.3	0.008	0.0015
22	1.951(5)	1.625(5)	1.3	0.009	0.0015
23	1.958(5)	1.639(5)	1.4	0.009	0.0018
24	1.967(5)	1.652(5)	1.6	0.009	0.0018
25	1.976(5)	1.668(5)	1.6	0.009	0.0018
28	2.000(5)	1.675(5)	0.9	0.007	0.0019
29	2.007(5)	1.662(5)	0.8	0.007	0.0020
30	2.011(5)	1.654(5)	0.7	0.006	0.0024
31	2.013(5)	1.652(5)	0.6	0.006	0.0025

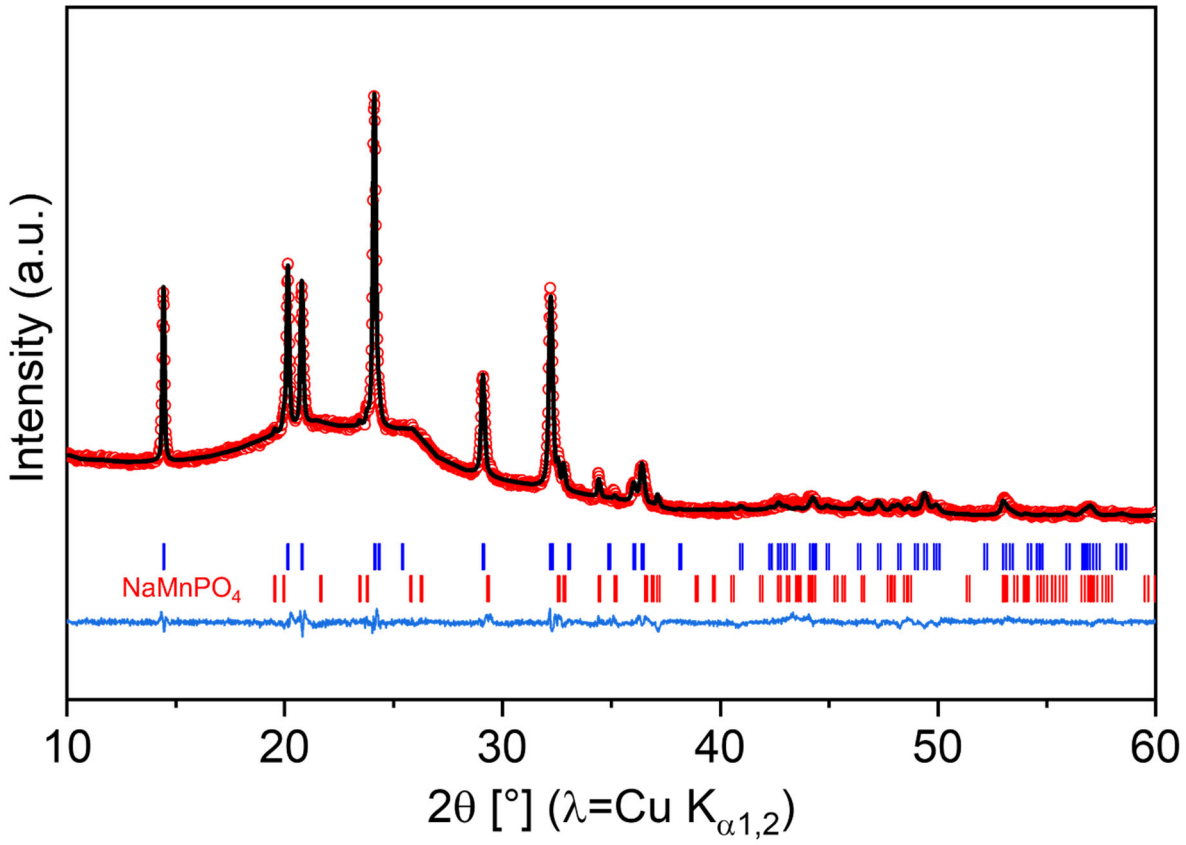

Figure S11. Rietveld refinement results of the XRPD pattern obtained from $Na_4MnV(PO_4)_3$ electrode charged at 4.3 V after 5 cycles with the voltage window of 2-4.3 V.

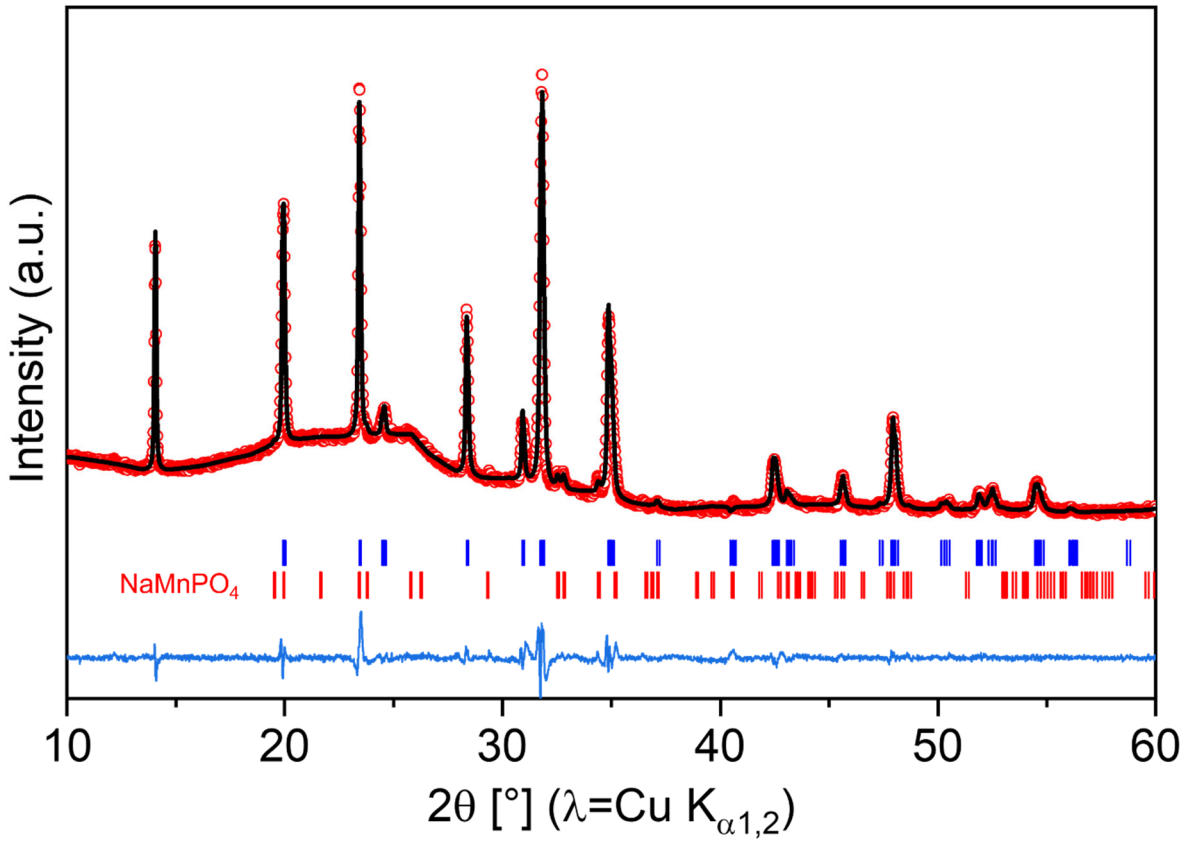

Figure S12. Full pattern matching analysis of the XRPD pattern obtained from $Na_4MnV(PO_4)_3$ electrode discharged at 2.0 V after 5 cycles with the voltage window of 2-4.3 V.